Chinese Chemical Letters 37 (2026) 112222

Contents lists available at ScienceDirect

Chinese Chemical Letters

journal homepage: www.elsevier.com/locate/cclet

Water-dispersible cyclen-based porous organic polymers for CO_2 direct air capture and photoreduction

Jiawei Hu, Qiao-Yan Qi, Qingxuan Tang, Wen-Zhuang Wang, Zhan-Ting Li*, Jia Tian*

State Key Laboratory of Organometallic Chemistry and Shanghai Hongkong Joint Laboratory in Chemical Synthesis, Shanghai Institute of Organic Chemistry, University of Chinese Academy of Sciences, Chinese Academy of Sciences, Shanghai 200032, China

ARTICLE INFO

Article history:
Received 21 July 2025
Revised 21 November 2025
Accepted 5 December 2025
Available online 5 December 2025

Keywords:
Porous organic polymers
Cyclen
Water-dispersible
Direct air capture
CO_2 photoreduction

ABSTRACT

Porous organic polymers (POPs) are promising candidates for CO_2 capture and conversion, yet the integration of direct air capture (DAC) and *in situ* conversion presents a fundamental challenge. Here, we report six novel water-dispersible cyclen-based POPs for efficient atmospheric CO_2 capture and photoreduction. The resulting POPs (**POP-1~6**) exhibit exceptional aqueous-phase CO_2 uptake (264–569 mg/g) with DAC capacities reaching 11–49 $mg\,g^{-1}\,d^{-1}$. When integrated with an iron porphyrin catalyst (**Fe-P**) and a ruthenium-based photosensitizer, these POPs enable efficient photocatalytic atmospheric CO_2-to-CO conversion with rates of 1.4–4.5 $\mu mol\,g^{-1}\,h^{-1}$ and a yield up to 93 % in water. These findings provide valuable insights for the further exploration of POP materials for atmospheric CO_2 capture and photoreduction.

© 2026 Published by Elsevier B.V. on behalf of Chinese Chemical Society and Institute of Materia Medica, Chinese Academy of Medical Sciences.

While carbon dioxide (CO_2) is the primary driver of anthropogenic climate change [1], its role as a key C1 feedstock necessitates the capture and conversion of atmospheric CO_2 to value-added chemicals [2–4]. However, the inherent ultradilute atmospheric CO_2 concentration (~400 ppm) fundamentally limits the conversion efficiency [1]. Carbon capture, utilization and storage (CCUS) technologies are critical to this effort [5], with direct air capture (DAC) emerging as an essential negative emissions solution [6–9]. Among various conversion strategies, CO_2 photoreduction offers a promising solution with minimal carbon footprint and environmental compatibility *versus* enzymatic, thermal, or electrochemical routes [10–12]. This challenge motivates the discovery of novel materials for integration of CO_2 DAC with photoreduction in one body for practical CCUS [13].

Porous materials are pivotal to DAC advancement through their tunable structures and functionalities [6,7]. The porous material systems, including porous carbons [14], zeolites [15], metal-organic frameworks (MOFs) [16–24], covalent-organic frameworks (COFs) [25,26], and porous organic polymers (POPs) [4,8,9], have been developed for integrated CO_2 capture-conversion [2–4]. Among them, the POPs exhibit exceptional structural diversity, featuring high surface areas, robust stability, tunable porosity, and facile functionalization [27], establishing them as ideal atmospheric CO_2 capture platforms [28]. Their customizable structures and pore environments further position POPs as scaffolds for integration of photocatalysts for CO_2 reduction [29–31]. To enhance CO_2 adsorption within POP materials, amine functionalization represents a key strategy where surface-grafted groups significantly boost CO_2 affinity [32–34]. The challenges in atmospheric CO_2 capture and conversion using POPs include [2,10,35–39]: (i) Intrinsically limited adsorption/conversion efficiency at ultradilute CO_2 concentrations due to poor interfacial contact; (ii) Performance degradation from poor material stability hindering adsorption-conversion functionality; (iii) System integration complexities involving adsorbent-catalyst coupling, CO_2 diffusion optimization, pore-blocking prevention, and incompatible operating conditions. Water-dispersible POPs, as an emerging class of porous materials [39], offer exceptional aqueous dispersibility, robust structural stability, and facile postsynthetic modification, which may resolve the integration challenges of CO_2 capture and conversion.

Herein, we synthesized six novel water-dispersible POPs of **POP-1~6** *via* polymerization of cyclen and tetrakis(4-(bromomethyl)phenyl)methane, followed by amine functionalization to enhance CO_2 affinity. The **POP-1~6** possessed excellent aqueous-phase dispersibility for efficient CO_2 DAC, which can further integrate with an Fe-porphyrin catalyst (**Fe-P**) and Ru-photosensitizer for efficient atmospheric CO_2 photoreduction to CO with a yield up to 93 %. This work establishes a dual-function material platform for integrated atmospheric CO_2 capture and photoreduction under ambient conditions.

* Corresponding authors.
E-mail addresses: ztli@mail.sioc.ac.cn (Z.-T. Li), tianjia@sioc.ac.cn (J. Tian).

https://doi.org/10.1016/j.cclet.2025.112222
1001-8417/© 2026 Published by Elsevier B.V. on behalf of Chinese Chemical Society and Institute of Materia Medica, Chinese Academy of Medical Sciences.

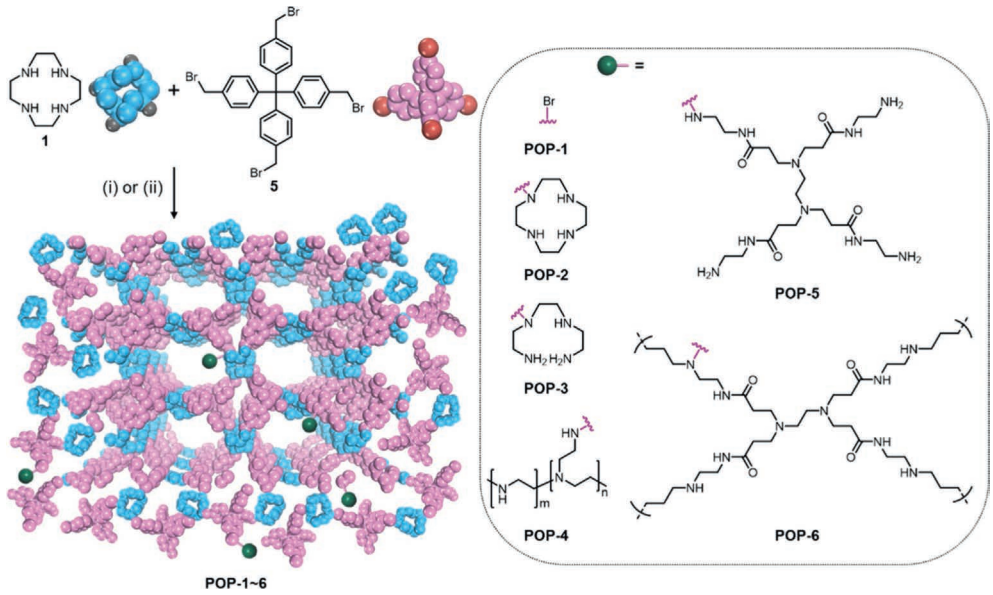


Fig. 1. Synthetic routes of designed POPs of **POP-1∼6** based on cyclen (**1**). (i) Reaction condition that was used to form **POP-1** from cyclen (**1**) and tetrakis(4-(bromomethyl)phenyl)methane (**5**). (ii) Two-step reaction conditions that contains (i) and subsequent reaction conditions to form **POP-2∼6** from **POP-1** by introducing cyclen (**1**), TETA, polyamine N7, PAMAM-G0 and a cross-linked network of polymer derived from the reaction of PAMAM-G0 and 1,3-diiodopropane *in situ*, respectively. The porous structure is simulated by Materials Studio 7.0. Blue, grey, purple, reddish brown, and dark green represent the skeleton of **1**, hydrogen atom of secondary amines of **1**, skeleton of **5**, bromine atom of **5**, bromine residue and amines, respectively. The purple bond only represents one plausible connection between the amine groups and the POP skeleton.

The 1,4,7,10-tetraazacyclododecane (cyclen, **1**) is one kind of microcyclic tetramine that can be used as an excellent node molecule for constructing POPs due to its inexpensiveness, good water solubility, and the amine groups of cyclen can potentially endow the POP with CO_2 adsorption properties [40]. Aiming to achieve flexible adsorption due to the interaction of amine groups with CO_2 [41], we employed **1** as an amine-based structural linker and tetrakis(4-(bromomethyl)phenyl)methane (**5**) as a node molecule to synthesize the first cyclen-based **POP-1** (Fig. 1, Figs. S1 and S2, and Method in Supporting information). As amine functionalization has been reported as an effective strategy to boost CO_2 affinity [32–34], we further introduced five selective primary and/or secondary amines to enhance the CO_2 adsorption capability. The **POP-2∼6** were synthesized based on the post-modification of **POP-1** with a series of added amines (Fig. 1 and Fig. S1). Specifically, we introduced cyclen to construct **POP-2**, *N*,*N*-di(2-aminoethyl)ethylenediamine (TETA) to construct **POP-3**, polyamine N7 to construct **POP-4**, PAMAM-G0 to construct **POP-5**, and a cross-linked polymer derived from the polymerization reaction of PAMAM-G0 and 1,3-diiodopropane *in situ* to construct **POP-6** (Fig. 1 and Fig. S1). To the best of our knowledge, these are the first examples of construction of cyclen-based POPs, and the resulting **POP-1∼6** exhibit excellent dispersibility in aqueous phase (Fig. S3 in Supporting information).

Fourier transform infrared (FT-IR) spectroscopy was executed to examine the chemical structure of **POP-1**. As shown in Fig. S4 (Supporting information), no absorption band at 3327 and 3276 cm^{-1} (N–H stretching vibration) manifests full conversion of secondary amine groups of **1**. The absorption band at 1019 cm^{-1} corresponding to C–N stretching vibration of tertiary amine group [42] further confirmed the formation of the new C–N bond in **POP-1**. Next, the absorption band at 2363 cm^{-1} corresponding to N–H stretching vibration of tertiary ammonium salt (N^+-H) was also observed, while the absorption at ∼1500 and 900 cm^{-1} (C–N^+ stretching vibration) for quaternary ammonium salt was absent [43–45]. Consistently, solid-state ^{13}C magic angle spinning nuclear magnetic resonance spectroscopy (^{13}C MAS NMR) of **POP-1** displayed a new peak assigned to the –CH_2– moieties at chemical shifts (δ) of 64.7 ppm, which further confirmed the formation of a new benzyl carbon (C–N) bond in **POP-1** (Fig. S11 in Supporting information) [4,46–48]. The FTIR and ^{13}C MAS NMR results confirmed the successful construction of **POP-1**. Notably, a week absorption peak at 615 cm^{-1} corresponding to C-Br stretching vibration in **POP-1** indicates that the residue of active benzyl bromide, which enables the post-modification with added amines (Fig. S4 in Supporting information). Next, elemental analysis was conducted to determine the residual amount of active benzyl bromide and the proportion of tertiary amine and tertiary ammonium salt in **POP-1** by ion exchange (Fig. S12 and Method in Supporting information). The result shows that **POP-1** contains 0.2 % (mass fraction) of unreacted bromine residues (C-Br) and 11.8 % (mass fraction) of ionic bond of bromine (Br^-), and the molar proportion of tertiary amine in **POP-1** is *ca.* 74 % and the cationic tertiary ammonium salts is *ca.* 26 % (Method in Supporting information). This cationic structure of **POP-1** enables the loading of anionic catalysts through electrostatic interaction [49]. Nuclear magnetic resonance (NMR) spectroscopy was also used to analyze the structure of **POP-1** and polyamines post-modified POPs of **POP-2∼6**. Liquid-state ^1H NMR spectroscopy showed only solvent peaks of POPs of **POP-1∼6** (Figs. S5∼S10 in Supporting information) due to their poor solubility, which is limited to structural verification of solid material, but ^1H NMR further confirmed no starting materials and no depolymerization products of **1** and **5** existed in **POP-1** (Fig. S5) and no residual free amines from starting materials and no depolymerization products of **1** and **5** existed in POPs of **POP-2∼6** (Figs. S6∼10).

The predicted three-dimensional model of **POP-1** with ideally ordered structure suggests that the pore size is approximately 1.0 nm as calculated by Materials Studio 7.0 (Fig. 1). Next, we performed the N_2 adsorption/desorption experiments to characterize the porosity of **POP-1**. The N_2 sorption isotherms displayed steep gas uptake at low relative pressures (Fig. S13a in Supporting information) with an adsorption capacity of 67.8 mg/g. The Brunauer-Emmett-Teller (BET) surface area of **POP-1** was calculated to be 19.8 m^2/g. Pore size distribution (PSD) analysis revealed that the

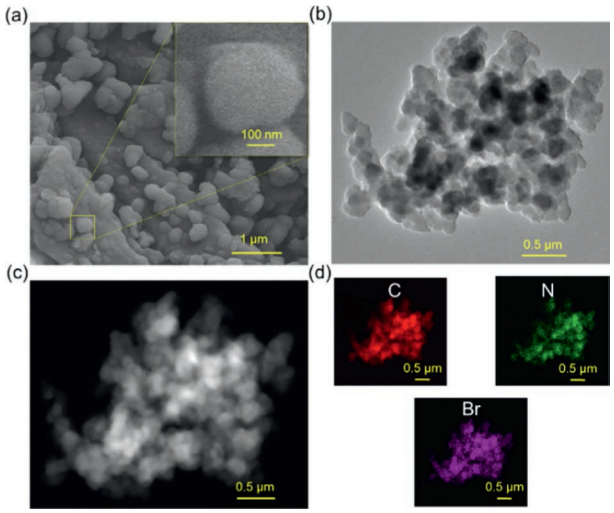


Fig. 2. Characterization of the morphology and composition of **POP-1**. (a) SEM image of **POP-1**. (b) TEM image of **POP-1** at 0.5 μm. (c) STEM image of **POP-1** at 0.5 μm, and (d) EDX mapping analysis of C, N, and Br of **POP-1**. Samples were prepared by drop-casting ~10 μL of the POP dispersed solution onto a carbon-coated copper grid.

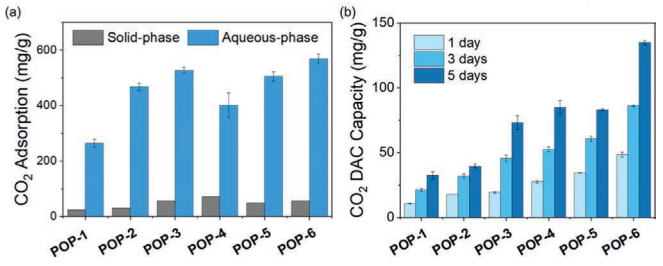


Fig. 3. (a) Saturated CO_2 adsorption capacities of **POP-1~6** in solid phase measured by CO_2 isothermal analysis (Fig. S17 and details in Supporting information) and in aqueous phase measured by GC (Table 1). (b) Atmospheric CO_2 adsorption capacities of POPs of **POP-1~6** in aqueous phase measured by GC, see Table 1 and Supporting information.

aperture distribution of **POP-1** is mostly at a range of 1–5 nm and contained both micropores (0.6–2 nm) and mesopores (2–35 nm) (Fig. S13b in Supporting information), the average pore width was calculated to be 1.8 nm with pore volume of 0.05 cm^3/g (Fig. S13). The hierarchical porous structure is expected to accelerate mass transport during CO_2 adsorption processes [2,4,10]. The scanning electron microscopy (SEM) and transmission electron microscopy (TEM) images showed that **POP-1** has an irregular, cross-linked, sponge-like porous structure (Fig. 2 and Fig. S14 in Supporting information). And the **POP-2~6** has the similar morphology as **POP-1** as revealed by TEM (Fig. S14 in Supporting information). Moreover, the scanning transmission electron microscopy (STEM) and energy dispersive X-ray (EDX) mapping analysis also certified the colocalization of C, N, and Br elements within of **POP-1~6** (Fig. 2, Figs. S14 and S15 in Supporting information). Small-angle X-ray scattering (SAXS) profile indicated an amorphous morphology of **POP-1** (Fig. S16 in Supporting information). Thermal gravimetric analysis (TGA) suggested that **POP-1~6** exhibited high thermal endurance that maintained structural integrity below 200 °C under inert conditions (Fig. S17 in Supporting information).

We first studied the solid-phase CO_2 adsorption capacities of **POP-1~6** by collecting the CO_2 isothermals at 298 K. The solid-phase CO_2 adsorption capacities were determined to be 24.4, 31.2, 56.5, 71.4, 49.2, and 56.9 mg/g, respectively (Fig. 3a, Fig. S18, Table 1 and Table S1 in Supporting information). However, the CO_2 isothermals only reflect the adsorption capacity in solid phase;

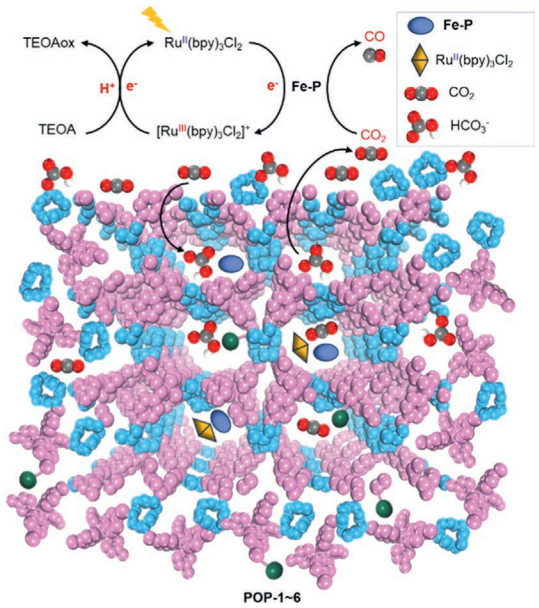


Fig. 4. The model illustration of the POP catalytic platform for atmospheric CO_2 photoreduction using **Fe-P** as catalyst, $Ru(bpy)_3Cl_2$ as photosensitizer, and TEOA as a sacrificial reagent in water.

there is still a lack of methods to determine CO_2 adsorption capacity in solution [27]. Given that the designed potential application of **POP-1~6** is to capture atmospheric CO_2 in aqueous phase, we developed a method to determine CO_2 adsorption capacity in water using gas chromatography (GC) (see Supporting information for details) [50]. The capacities of CO_2 adsorption of **POP-1~6** were determined to be 263.9, 467.9, 527.2, 401.6, 505.1, and 569.1 mg/g, respectively (Fig. 3a, Table 1 and Table S1). We then explored the application of **POP-1~6** for CO_2 DAC by continuously pumping air into well-dispersed POPs in aqueous phase for 1–5 days. The CO_2 DAC capacities of **POP-1~6** over 5 days in aqueous phase were determined to be 10.8, 17.9, 19.5, 27.6, 34.3, and 48.5 mg g^{-1} d^{-1}, respectively (Fig. 3b, Table 1, and Table S1). The significant difference in the ability of solid materials to adsorb CO_2 in air *versus* in aqueous environments may primarily be attributed to the distinct roles of water molecules in the adsorption process. The fundamental cause lies in the inherent differences in the physical state, concentration, mass transfer kinetics, and adsorption or reaction mechanisms of CO_2 across different media. In air, adsorption involves the interaction between low-concentration gaseous CO_2 and solid materials; in contrast, in aqueous solutions, it entails the interaction between dissolved CO_2 species, including carbonic acid, bicarbonate, and carbonate ions, and the solid material within a hydrated environment [51–53]. The enhanced CO_2 adsorption capacities of **POP-2~6** compared to **POP-1** may be attributed to the successful post-modification of additional amines, which the activated amine sites at aperture would draw more CO_2 molecules into the pores [54–56]. The comparisons of CO_2 capture performance of **POP-1~6** with a range of benchmark materials are summarized in Tables S2 and S3 (Supporting information) [57].

We then investigated the catalytic activity of **POP-1~6** when integrated with catalysts by a series of photocatalytic experiments. The CO_2 photoreduction experiments were conducted using 5,10,15,20-tetrakis(4-sulfonatophenyl)porphyrin iron(III) chloride (**Fe-P**) as a catalyst, $Ru(bpy)_3Cl_2$ as a photosensitizer, and TEOA as a sacrificial reagent in the POP system (Fig. 4 and Fig. S19 and Table S4 in Supporting information for details). The **Fe-P** and $Ru(bpy)_3Cl_2$ were integrated with **POP-1~6** to achieve the photocatalytic CO_2 conversion. The density functional theory (DFT)

Table 1
Comparison of the CO_2 adsorption capacities of **POP-1∼6**.

POPs	CO_2 adsorption capacity (298 K, 1 atm CO_2[a], mg/g)		CO_2 DAC capacity in aqueous phase (298 K, 1 atm air, mg/g)		
	Solid-phase	Aqueous-phase	1 d[b]	3 d	5 d
POP-1	24.4[c]	263.9 ± 14.7	10.8 ± 0.4	21.4 ± 1.2	32.5 ± 3.0
POP-2	31.2	467.9 ± 12.9	17.9 ± 0.1	32.0 ± 1.7	39.6 ± 1.4
POP-3	56.5	527.2 ± 10.5	19.5 ± 0.7	45.6 ± 2.5	73.2 ± 5.4
POP-4	71.4	401.6 ± 44.3	27.6 ± 0.9	52.6 ± 1.8	84.9 ± 5.4
POP-5	49.2	505.1 ± 17.1	34.3 ± 0.3	60.8 ± 2.2	83.0 ± 0.8
POP-6	56.9	569.1 ± 16.8	48.5 ± 2.0	86.2 ± 0.6	134.9 ± 1.7

[a] 1 atm refers to one standard atmosphere, which is defined as the pressure exerted by the weight of the Earth's atmosphere at sea level under standard conditions.
[b] 1 day refers to 24 h.
[c] The general formula for conversion between mg/g and mmol/g is: mg/g = mmol/g × 44.01, where 44.01 is the molar mass of CO_2.

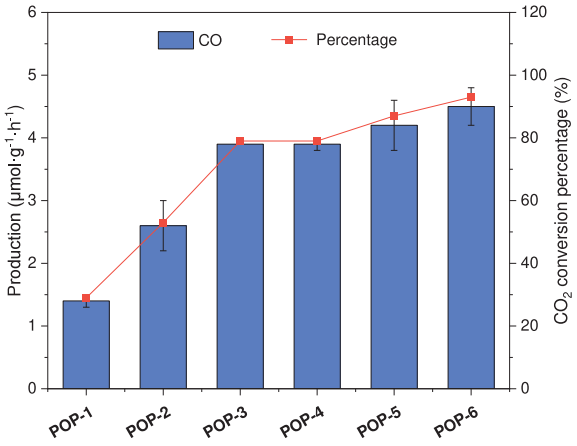


Fig. 5. The atmospheric CO_2 photoreduction performance of **POP-1∼6** using 0.01 mmol/L of **Fe-P**, 10 mmol/L of $Ru(bpy)_3Cl_2$, and 20 mmol/L of TEOA in water under an air atmosphere (The atmospheric CO_2 concentration was determined to be 408.6 ± 2.9 ppm).

calculations confirmed that the energy levels of the $Ru(bpy)_3Cl_2$ photosensitizer matched with those of the **Fe-P** catalyst, and the electron transfer was allowed (Fig. S20 in Supporting information). The ^{13}C isotope labelling experiment confirmed that the produced CO was from the photoreduction of CO_2 (Fig. S21 in Supporting information). The reaction conditions were then systematically studied and optimized for CO productivity and the turnover number (TON) using different contents of POP, the concentration of the $Ru(bpy)_3Cl_2$ photosensitizer, and the **Fe-P** catalyst (Fig. S22 and Tables S5∼S7 in Supporting information for details). Next, we studied the atmospheric CO_2 photoreduction of **POP-1∼6** (1 mg/mL) using 0.01 mmol/L of **Fe-P**, 10 mmol/L of $Ru(bpy)_3Cl_2$, and 20 mmol/L TEOA, in water under an air atmosphere. The results showed that the **POP-1∼6** can achieved CO_2-to-CO conversion with a productivity of 1.4 μmol g^{-1} h^{-1} (TON = 335, yield = 29 %), 2.6 μmol g^{-1} h^{-1} (TON = 622, yield = 53 %), 3.9 μmol g^{-1} h^{-1} (TON = 928, yield = 80 %), 3.9 μmol g^{-1} h^{-1} (TON = 927, yield = 79 %), 4.2 μmol g^{-1} h^{-1} (TON = 1015, yield = 87 %), and 4.5 μmol g^{-1} h^{-1} (TON = 1085, yield = 93 %), respectively (Fig. 5, Table 2 and Table S8 in Supporting information). The high atmospheric CO_2 photoreduction performance of **POP-3∼6** may be owed to their high CO_2 adsorption capacities and the interactions, such as hydrophobic effect and electrostatic interactions, between the POP scaffolds and the **Fe-P** catalyst [58]. The cross-linked networks and hierarchical porous structure of POPs might also optimize the CO_2 mass transfer, electron transport, and the stability of intermediates [58]. We further performed photocatalytic recycling experiments of **POP-1∼6**. The recycling results showed that these POPs have good recyclability with negligible activity loss after five catalytic cycles (Fig. S23 and Table S9 in Supporting information). The FT-IR

Table 2
Comparison of atmospheric CO_2 photoreduction performance of **POP-1∼6** (see Supporting information and Table S5 for details).

POPs	CO_2 conversion (%)[a]	CO productivity (μmol g^{-1} h^{-1})	TON
POP-1	29	1.4 ± 0.1	335 ± 18
POP-2	53	2.6 ± 0.4	622 ± 92
POP-3	80	3.9 ± 0.0	928 ± 1
POP-4	79	3.9 ± 0.1	927 ± 27
POP-5	87	4.2 ± 0.4	1015 ± 90
POP-6	93	4.5 ± 0.3	1085 ± 75

[a] The percentage of atmospheric CO_2 conversion is defined as the ratio of the output of CO to the initial amount of atmospheric carbon dioxide (CO_2). The concentration of atmospheric CO_2 was determined to be 408.6 ± 2.9 ppm.

experiments showed no obvious changes for **POP-1** before and after five photocatalytic cycles, which indicated that its structural integrity was maintained (Fig. S24 in Supporting information).

Meanwhile, the BET results showed that there is no obvious surface area loss in recycled **POP-1** after photocatalytic recycling, possibly due to no pore collapse or blockage (Fig. S13). XRD analysis showed that **POP-1∼6** and recycled **POP-1∼6** both are amorphous materials and have no obvious structure change (Fig. S25 in Supporting information). The scanning transmission electron microscopy (STEM) and energy dispersive X-ray (EDX) mapping analysis also certified the incorporation of heteroatoms of N and Br elements within of **POP-1∼6** and of N, Br, Fe and Ru elements within recycled **POP-1∼6** (Fig. 2, Figs. S14, S15 and S26, and Table S10 in Supporting information). The quantitative EDS analysis (weight% and atomic%, Table S10) for all catalysts (**POP-1∼6**) also confirmed their stability after reuse since the element contents of C and N remain basically unchanged. XPS analysis of recycled **POP-1** confirmed the exist of C–C and C–N (Fig. S27 in Supporting information) [59–64], and there is no obvious signal of Fe and Ru may due to their trace amount (Figs. S15 and S26 and Table S10) [59–64]. The comparison of CO_2 reduction performance of these **POP-1∼6** platforms with a range of benchmark materials for integrated CO_2 DAC and photoreduction are summarized in Table S11 (Supporting information).

In summary, we developed six amine-functionalized, water-dispersible cyclen-based POP platforms for atmospheric CO_2 capture and photoreduction. The **POP-1∼6** exhibit exceptional aqueous-phase CO_2 uptake 264–569 mg/g, with DAC capacities reaching 11–49 mg g^{-1} d^{-1} in water. When integrated with photocatalysts, the **POP-1∼6** can achieve atmospheric CO_2-to-CO conversion with a productivity of 1.4–4.5 μmol g^{-1} h^{-1} and CO_2 conversion rates up to 93 % compared to free molecules while maintaining stability and recyclability (>5 cycles). The design principles demonstrated herein provide insights for creating integrated capture-conversion systems based on POPs advancing carbon neutrality goals.

CRediT authorship contribution statement

Jiawei Hu: Writing – original draft, Formal analysis, Data curation. **Qiao-Yan Qi:** Data curation. **Qingxuan Tang:** Data curation. **Wen-Zhuang Wang:** Data curation. **Zhan-Ting Li:** Supervision, Conceptualization. **Jia Tian:** Writing – review & editing, Writing – original draft, Supervision, Project administration, Investigation, Funding acquisition, Conceptualization.

Declaration of competing interest

The authors declare that they have no known competing financial interests or personal relationships that could have appeared to influence the work reported in this paper.

Acknowledgments

We acknowledge the support from the National Key Research and Development Program of China (No. 2024YFA1510600), the National Natural Science Foundation of China (No. 22271306), the Strategic Priority Research Program of the Chinese Academy of Sciences (Nos. XDB0610000, XDA0540000), the Shanghai Rising-Star Program (No. 22QA1411200), the Shanghai Institute of Organic Chemistry and the Shanghai Branch, Chinese Academy of Sciences. We acknowledge the support from the National Key Research and Development Program of China (No. 2022YFA1206200). Jia Tian acknowledges the Shanghai Synchrotron Radiation Facility (SSRF) of BL16B1 (No. 31124.02.SSRF.BL16B1) and BL10U1 (No. 31124.02.SSRF.BL10U1) for the assistance on SAXS or USAXS and the SSRF Key Research Project (No. 2023-SSRF-ZD-503466). We thank Prof. Zhi Ma, Dr. Kun Cui and Qiaoling Zhao in Analysis and Testing Center of SIOC-CAS for assistance in SEM and TEM measurements. The AI-driven experiments, simulations and model training were performed on the robotic AI-Scientist platform of Chinese Academy of Sciences.

Supplementary materials

Supplementary material associated with this article can be found, in the online version, at doi:10.1016/j.cclet.2025.112222.

References

[1] R. Monastersky, Nature 497 (2013) 13–14.
[2] Z. Zhong, X. Wang, B. Tan, Chem. Eur. J. 31 (2025) e202404089.
[3] Q. Cheng, M. Huang, Q. Ye, et al., Chin. Chem. Lett. 35 (2024) 109112.
[4] J.K. Tang, C.Y. Zhu, T.W. Jiang, et al., J. Mater. Chem. A 8 (2020) 18677–18686.
[5] H. Chu, Z. Huang, Z. Zhang, et al., Sep. Purif. Technol. 343 (2024) 127153.
[6] X. Zhu, W. Xie, J. Wu, et al., Chem. Soc. Rev. 51 (2022) 6574–6651.
[7] Y. Zhang, L. Ding, Z. Xie, et al., Chin. Chem. Lett. 36 (2025) 109676.
[8] Y. Bao, J. Liu, Y. Zhang, et al., Fuel 331 (2023) 125909.
[9] C. He, H. Yang, L. Fu, Chin. Chem. Lett. 34 (2023) 107581.
[10] K.S. Song, P.W. Fritz, A. Coskun, Chem. Soc. Rev. 51 (2022) 9831–9852.
[11] Y. Li, Y. Wei, W. He, et al., Chin. Chem. Lett. 34 (2023) 108417.
[12] J. Zhou, H. Liu, H. Wang, Chin. Chem. Lett. 34 (2023) 107420.
[13] X. Gao, G. Yan, M. Li, et al., Fuel 378 (2024) 132960.
[14] L. Shao, S. Wang, M. Liu, et al., Chem. Eng. J. 339 (2018) 509–518.
[15] C. Chen, D.W. Park, W.S. Ahn, Appl. Surf. Sci. 292 (2014) 63–67.
[16] F.F. Yang, Y.K. Ding, L.K. Wu, et al., Chin. Chem. Lett. 36 (2025) 110550.
[17] J. Liu, C. Chen, K. Zhang, et al., Chin. Chem. Lett. 32 (2021) 649–659.
[18] X.D. Zhang, J.M. Huang, X. Zhu, et al., Chin. Chem. Lett. 36 (2025) 109937.
[19] X. Wu, J. Lu, Z. Zhu, et al., Chin. Chem. Lett. 36 (2025) 110151.
[20] L. Chen, Q. Liu, J. Yang, et al., Chin. Chem. Lett. 34 (2023) 107335.
[21] X. Zhang, Y. Zhang, W. Zhou, et al., Chin. Chem. Lett. 34 (2023) 107368.
[22] A.A. Zhang, R. Wang, H.B. Huang, et al., Chin. Chem. Lett. 34 (2023) 107311.
[23] X. Dong, Z. Xie, D. He, et al., Chin. Chem. Lett. 34 (2023) 107459.
[24] X. Kang, G. Fu, X.Z. Fu, et al., Chin. Chem. Lett. 34 (2023) 107757.
[25] Z. Zhou, T. Ma, H. Zhang, et al., Nature 635 (2024) 1–6.
[26] Z. Gu, Z. Shan, Y. Wang, et al., Chin. Chem. Lett. 35 (2024) 108356.
[27] H. Gao, Q. Li, S. Ren, Curr. Opin. Green Sustain. Chem. 16 (2019) 33–38.
[28] N. Huang, G. Day, X. Yang, et al., Sci. China Chem. 60 (2017) 1007–1014.
[29] J. Li, K. Ma, Y. He, et al., Catal. Sci. Technol. 11 (2021) 7300–7306.
[30] W.J. Wang, K. Chen, Chin. Chem. Lett. 36 (2025) 109998.
[31] G. Xu, Q.L. Hong, Y. Sun, et al., Chin. Chem. Lett. 33 (2022) 2915–2918.
[32] T. Shi, Z. Wu, Z. Wu, et al., J. Polym. Sci. 62 (2024) 1554–1568.
[33] R. Wang, S. Wang, C. Zhu, et al., Chin. Chem. Lett. 36 (2025) 111547.
[34] X. Kong, S. Li, M. Strømme, et al., Nanomaterials 9 (2019) 1020.
[35] M. He, H. Zhao, J. Jia, et al., Environ. Res. 267 (2025) 120701.
[36] Q.H. Zheng, C. Chen, S.M. Cao, et al., Chin. Chem. Lett. 34 (2023) 107273.
[37] C. Cui, G. Li, Z. Tang, Chin. Chem. Lett. 32 (2021) 3307–3321.
[38] S.B. Yu, F. Lin, J. Tian, Chem. Soc. Rev. 51 (2022) 434–449.
[39] X. Hong, Y. Fang, D. Chao, Mol. Catal. 549 (2023) 113476.
[40] M. Meyer, V. Dahaoui-Gindrey, C. Lecomte, Coord. Chem. Rev. 178-180 (1998) 1313–1405.
[41] Q.M. Sun, J.H. He, J.M. Lu, Energy Sci. Eng. 11 (2023) 952–973.
[42] R. Gomes, A. Bhaumik, J. Solid State Chem. 222 (2015) 7–11.
[43] M.E. Atlaskina, A.A. Atlaskin, O.V. Kazarina, Environments 8 (2021) 134.
[44] Z. Xiao, D. Kong, J. Liang, Carbon 116 (2017) 633–639.
[45] Z.H. Ping, Q.T. Nguyen, S.M. Chen, Polymer 42 (2001) 8461–8467.
[46] L. Zhang, N. Di, Z. Wang, et al., J. Membr. Sci. 688 (2023) 122129.
[47] W. Cao, Z. Wang, Q. Zeng, et al., Appl. Surf. Sci. 389 (2016) 404–410.
[48] K. Zhang, X.J. Chen, AIP Adv. 8 (2018) 025004.
[49] Z.W. Liu, B.H. Han, Curr. Opin. Green Sustain. Chem. 16 (2019) 20–25.
[50] R.M. Enick, S.M. Klara, Chem. Eng. Commun. 90 (1990) 23–33.
[51] S.J. Datta, C. Khumnoon, Z.H. Lee, et al., Science 350 (2015) 302–306.
[52] N.L. Drenchev, K.K. Chakarova, O.V. Lagunov, et al., J. Vis. Exp. 156 (2020) e60285.
[53] J. Wang, L. Huang, R. Yang, et al., Energy Environ. Sci. 7 (2014) 3478–3518.
[54] R. Ahmadi, M.S. Alivand, N.H. Mohammad Hossein Tehrani, et al., Chem. Eng. J. 415 (2021) 129076.
[55] H. Jung, S. Jeon, D.H. Jo, et al., Chem. Eng. J. 307 (2017) 836–844.
[56] L. Zou, Y. Sun, S. Che, et al., Adv. Mater. 29 (2017) 1700229.
[57] M.G. Darmayanti, K.L. Tuck, S.H. Thang, Adv. Mater. 36 (2024) 2403324.
[58] H. Daglar, H.C. Gulbalkan, G.O. Aksu, et al., Adv. Mater. 36 (2024) 2405532.
[59] M.C. Biesinger, B.P. Payne, A.P. Grosvenor, et al., Appl. Surface Sci. 257 (2011) 2717–2730.
[60] N.S. McIntyre, M.G. Cook, Anal. Chem. 47 (1975) 2208–2213.
[61] A. Taylor, J. Chem. Technol. Biotechnol. 53 (1992) 215.
[62] S. Kumar, P. Chakrabortty, R.V. Singh, et al., ACS Appl. Energy Mater. 7 (2024) 4429–4444.
[63] S. Kumar, P. Chakrabortty, B. Banerjee, et al., ACS Appl. Nano Mater. 8 (2025) 12946–12956.
[64] P. Sarkar, A.H. Chowdhury, S. Biswas, et al., Mat. Today Chem. 21 (2021) 100509.